View metadata, citation and similar papers at core.ac.uk
brought to you by CORE
provided by Italian Group Fracture (IGF): E-Journals / Gruppo Italiano Frattura

DEVELOPMENT AND CHARACTERIZATION OF TiO_2 COATINGS PREPARED BY ELECTRIC ARC-PHYSICAL VAPOUR DEPOSITION SYSTEM

C. Giolli, G. Rizzi, A. Scrivani, R. Ferpozzi, S. Troglio, M. Muniz Miranda, A. Tolstoguzov, U. Bardi, F. Borgioli, A. Fossati, A. Credi, A. Di Fabio, S. Parmeggiani, A. Zoppi.

TiO_2 thin coatings were prepared, on various substrates, through evaporation of metallic titanium in an oxidizing atmosphere by modified electric arc physical vapor deposition (EA-PVD). The coatings were characterized chemically (by means of XPS and SIMS) and from the structural point of view (by means of XRD and Raman spectroscopy), in order to understand the factors which lead to homoge-neous coatings with high anatase content. The type of substrate is the main parameter that influence the crystal structure of the coatings: when stainless steel is used as substrate the coatings consist es-sentially of rutile, while on glass substrates coatings containing mainly anatase are obtained. The photocatalytic activity of the samples upon UVA irradiation was tested by using phenol as the target molecule. Phenol in the solution can be photocatalytically and rapidly degraded through the EA-PVD anatase TiO_2 coatings.

KEY WORDS:

INTRODUCTION

Titanium dioxide is a multifunctional material having many potential applications, such as medical technology, gas sensors and wear protection, owing to its favorable characteristics (physical and chemical stability and non-toxicity) [1]. As a semiconductor material, titanium dioxide has raised a great interest for its physicochemical properties that have led to many industrial applications [2]. The excitation of TiO_2 with photons with energy equal or greater than its band gap leads to the promotion of electrons in the conduction band and the concomitant formation of holes in the valence band.

Such photogenerated electron-hole pairs can cause redox reactions involving adventitious chemical species onto the surface of the semiconductor. The great oxidizing power of the holes generated by bandgap excitation, the chemical inertness and the lack of toxicity are the main reasons for the wide-spread use of TiO_2 as a photocatalyst.

Photocatalytic oxidation processes at the surface of titanium dioxide have been successfully employed for the degradation of organic molecules in the atmosphere (e.g., pollutants and compounds responsi-ble of bad smells) and in wastewater [3-6]. Therefore, titanium dioxide surfaces could be easily inte-grated in air heating, ventilation and conditioning systems. TiO_2 coatings supported on ceramic or glass could find many applications for their antibacterial, anti-fogging and self-cleaning properties [7].

Carlo Giolli, Gabriele Rizzi, Andrea Scrivani, Roberto Ferpozzi, Sergio Troglio
Vacuum Surtec s.r.l., San Polo di Torrile, Parma, Italy
Maurizio Muniz Miranda, Alexander Tolstoguzov, Ugo Bardi
Consorzio Interuniversitario Nazionale per la Scienza e Tecnologia dei Materiali (INSTM), Firenze, Italy
Francesca Borgioli, Alessio Fossati
Dipartimento di Ingegneria Civile, Università di Firenze, Firenze, Italy
Alberto Credi, Alberto Di Fabio, Silvia Parmeggiani
Dipartimento di Chimica "G. Ciamician", Università di Bologna, Bologna, Italy
Angela Zoppi
Dipartimento di Chimica, Università di Firenze, Sesto Fiorentino, Italy

A short version of this paper was presented at the 5th International Surface Engineering Congress (ISEC) and Exhibition, Seattle (USA), May 15-17 2006

Parameters / Sample number	Substrate	coating time (min)	BIAS (V)	Gas composition	Gas flux (referred to sample 1)	Gas pressure (referred to sample 1)	Arc control (EMCAS)	substrate temperature (°C)
1	copper	10	120	24%Ar/76%O_2	1.00	1.00	B	250
2	copper	10	120	100% O_2	0.95	0.40	A	250
3	copper	10	50	100% O_2	0.95	0.50	A	250
4	copper	10	0 - 120	100% O_2	0.95	0.50	A	150 - 300
5	copper	10	120	100% O_2	1.14	0.50	B	250
6	stainless steel	20	120	100% O_2	1.00	0.75	C	300
7	stainless steel	10	120	100% O_2	1.10	1.25	A	250
8A	stainless steel	10	0 - 120	100% O_2	0.97	0.50	B	150 - 300
8B	glass							
9A	stainless steel	15	0 - 120	100% 02	1.06	0.50	B	150 - 300
9B	glass							
10A	stainless steel	20	0 - 120	100% 02	1.11	0.50	B	150 - 300
10B	glass							

▲ *Tab. 1*

EA-PVD(EMCAS) deposition parameters for analyzed samples.

Parametri di deposizione EA-PVD(EMCAS) utilizzati per la preparazione dei rivestimenti analizzati.

The photocatalytic activity of TiO_2 depends mainly on its crystallographic structure. TiO_2 has three different stable crystalline structures: anatase, rutile and brookite. Anatase shows the highest photo-catalytic activity [8]. Various techniques are employed for the preparation of photoactive TiO_2 coat-ings, including sol-gel [9], chemical vapor deposition [10], atomic layer deposition [11], plasma im-mersion ion implantation [12], pulse laser deposition [13] and magnetron sputtering-physical vapor deposition [14]. The Electric Arc evaporating system (EA-PVD) [15] has several advantages in terms of fast deposition rates and good control of the process parameters in respect of conventional evapora-tion sources. In comparison with the high velocity oxy-fuel (HVOF) process [16] EA-PVD shows a lower deposition rate but the capability to coat very thin films of nanometric thickness [17]. This tech-nique was utilized in the present research in conjunction with an innovative Electro Magnetic Con-trolled Arc Stirring (EMCAS) device [18].

The aim of the present work was to produce TiO_2 thin coatings on various substrates using the EA-PVD technique and optimize the deposition parameters in order to obtain a good photocatalytic activ-ity. The samples were characterized from the chemical and crystallographic point of view for evaluat-ing the main EA-PVD deposition parameters that influence the characteristics of the coatings. Moreo-ver, the photocatalytic properties of the samples with respect to the degradation of a prototypical or-ganic molecule (phenol) in water were investigated.

EXPERIMENTAL PROCEDURES

EA-PVD (EA-EMCAS/PVD)

TiO_2 coatings were produced using a industrial EA-PVD coating apparatus, modified with a so called Electro Magnetic Controlled Arc Stirring (EMCAS) device. The EMCAS system is an electromagnetic device that controls the electric arc movement (scanning speed and scanning position), the dimension of electric arc spot, and the time of permanence of spot in a desired position on the target. In this way it is possible to control the plasma density, the plasma temperature, the target wear and the evaporation zone of the target.

The deposition apparatus has two separate and different electric circuits: 1) high voltage (up to 1000 V) and low current (< 5 A) for obtaining a plasma able to clean the substrates, and 2) relatively low voltages (5 - 30 V) and high currents (50 - 150 A) for coating the substrates; moreover, it is possible to apply to the substrates to be coated a negative bias.

In this work three different configuration of the EMCAS system, A, B and C (Tab. 1), were used. TiO_2 coatings were deposited changing the deposition parameters and the substrates. The complete deposition procedure is patented [13]. Besides the configuration of EMCAS device as described above, coating time, bias, substrates temperature, gas composition, flux and pressure were changed, as summarized in Tab. 1. The value of bias for the samples 4, 8, 9 and 10 floated between 0 and 120 V. Bias floating voltage influenced also the substrate temperature, which varied between 150 and 300°C, during the deposition process. The temperature of the samples surface, during the deposition process, was measured by a thermocou-

ple system in contact with the surface of the substrates. The values of bias and temperature for the other coated samples did not change significantly during the deposition process; the measured values are indicated in Tab. 1.
Specimens (50 x 5 mm; thickness: 2 mm) of copper, AISI 304L stainless steel and glass were used as substrates, as summarized in Table 1. Copper substrates were polished up to an average roughness (Ra) of 0.03 ± 0.01 μm, while stainless steel and glass substrates were sand blasted up to a Ra of 1.7 ± 0.3 Ìm and 5.3 ± 1.1 μm, respectively.

Characterization techniques

X-ray photoelectron spectroscopy (XPS) analysis was performed in an ultra-high vacuum (10^{-10} mbar) experimental system equipped with a VSW HAC 5000 hemispherical electron energy analyser and an Al Kα X-ray source. Photoelectron spectra were acquired in the constant-pass-energy mode at E_{pas} = 44 eV; the overall energy resolution was 1.2 eV measured as a full-width at half maxi-mum (FWHM) of the Ag 3d5/2 line of a pure silver reference. Details of the system have been reported in previous publications [19, 20]. In the spectra the peak positions were determined by curve fitting after Shirley background subtraction. The binding energies were measured in reference to the C 1s peak of the adventitious aliphatic carbon assumed to be at 285 eV.
Secondary ion mass spectrometry (SIMS) measurements were carried out in a high-vacuum (10^{-8} mbar) custom-built installation [21-23] based on standard commercial components. A duoplasmatron ion gun (model DP50B by VG Fison) generated mass-filtered 16O2+ primary-ion beam (about 150-170 nA) with a bombarding energy of 6 keV (3 keV/atom). The primary ions impinged on the surface at an angle of 30° with respect to the normal. The positive and negative secondary ions were measured by a Hiden EQS 1000 Mass Energy Analyser, which unifies a high-transmission electrostatic energy analyser and a powerful quadrupole-based mass filter. The primary beam was raster-scanned and eroded a sample area of about 250x250 μm^2. "Crater effect" was avoided with electronic gating of the registration system, since only secondary ions coming from central 20% area of the crater are measured. The depth of sputter craters was determined by a Tencor Stylus Profiler P-10. Micrographic examination was performed by ESEM QUANTA 200 FEI. Raman spectra were recorded us-ing the 514.5-nm line of an Ar^+ laser, a Jobin-Yvon HG2S monochromator equipped with a cooled RCA-C31034A photomultiplier with a 50-mW laser power. Power density measurements were per-formed with a power meter instrument (model 362; Scientech, Boulder, CO, USA) giving ~5% accuracy in the 300-1000 nm spectral range. Micro-Raman spectra were measured using a Renishaw RM2000 single grating spectrograph, coupled to a diode laser source emitting at 785 nm. Sample irra-diation was accomplished using a x50 microscope objective. The spatial resolution was about 1.5 μm. The beam power on the sample was 3 mW. Raman light was filtered by a double holographic Notch filters system and collected by an air-cooled CCD detector. The spectral resolution was about 3 cm-1. Calibration was obtained by acquiring the 520 cm^{-1} Raman line of a silicon wafer. Acquisition times were from 10 s to 100 s.
X-ray diffraction analysis was performed by means of a Philips PW1050/37 diffractometer in Bragg-Brentano configuration (Cu Kα radiation generated at 40 kV and 25 mA). Patterns were collected us-ing acquisition times up to 40 s/step in order to increase the signal-to-noise ratio. Diffraction patterns were analysed by means of the program MAUD using the Rietveld method [24]. Additional X-ray dif-fraction analysis was performed collecting the diffraction patterns in glancing angle configuration by using constant incident angles varied in the range 5-10°. Under these conditions the mean penetration depth (i.e. the depth at which the intensity drops by a factor of e) ranges from 1.18 μm (α = 5°) to 2.19 μm (α = 10°).

Photochemical experiments

The photocatalytic activity of the samples was evaluated by means of the analysis of the degradation of phenol in aqueous solution upon light irradiation of the coating. The coated substrates were cut in stripes of 6x30 mm such that they could be introduced into a quartz spectrofluorimetric cell (Hellma, 1.00 cm path length) filled with 2.50 ml of an aqueous solution containing $5.0x10^{-4}$ M phenol (Fluka). The solution was irradiated by a 125 W medium pressure mercury lamp (Helios Italquartz) with the UVA lines (334 and 365 nm), isolated by means of a cutoff filter (λ > 320 nm). Note that the visible lines of the medium pressure Hg lamp were present in the irradiation light, but were not ab-sorbed by TiO_2 whose cutoff wavelength in the case of the examined samples was around 370 nm. It is important to note that the above irradiation wavelengths were not absorbed by phenol because it does not show absorption bands at λ > 300 nm. Hence, any photodegradation caused by direct photo-excitation of phenol could be ruled out in our system, as confirmed by control irradiation experiments performed on a phenol solution in the absence of the TiO_2 sample. The concentration of phenol in the solution was monitored by absorption and, more conveniently, fluorescence spectroscopy by means of a Perkin Elmer λ40 spectrophotometer and a LS50 spectrofluorimeter. The fluorescence of the phenol was monitored at 300 nm upon excitation at 270 nm; in the conditions employed the concentration is linearly related to the luminescence intensity [25]. During irradiation the solution was continuously stirred by means of a magnetic stirrer. The irradiance of the light source in the UVA region was on the order of 3.8 mW/cm^2 (by comparison, the average irradiance of sunlight in the same spectral region is on the order of 4 mW/cm^2 [26]).

RESULTS AND DISCUSSION

TiO_2 on copper

Five TiO_2 coatings were prepared on copper substrates at different conditions, as described in Tab. 1. The thickness and the relative calculated rate of deposition, as measured by SIMS and profilometry, are summarized in Tab. 2.
As an example, the XPS spectrum of sample 3 is shown in Fig. 1 (a).

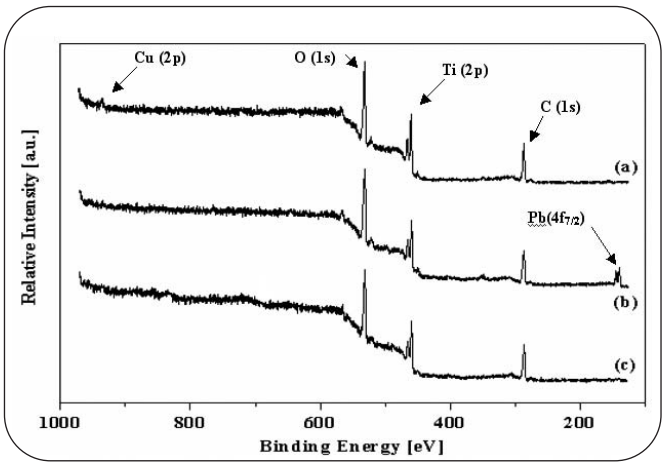

Fig. 1

XPS spectra of TiO_2 on copper (sample 3) (a) and on stainless steel (samples 6 (b) and 8A (c)).
Spettri XPS dei campioni di TiO_2 su rame (sample 3) (a) e su acciaio inox (samples 6 (b) and 8A (c)).

Sample number	Substrate	Raman	GA XRD	Thickness (nm)	Deposition Rate (nm/min)
1	copper	anatase	–	60-80	6-8
2	copper	anatase	–	700-750	70-75
3	copper	anatase	–	280-330	28-33
4	copper	anatase	–	840-890	84-89
5	copper	anatase	–	580-630	58-63
6	stainless steel	–	anatase/rutile	350-400	18-20
7	stainless steel	–	rutile	250-300	25-30
8A	stainless steel	rutile	–	400-450	40-45
8B	glass	anatase/amorphous	–	400-450	40-45
9A	stainless steel	rutile	–	750-800	50-55
9B	glass	anatase	–	750-800	50-55
10A	stainless steel	rutile	rutile	1100-1200	55-60
10B	glass	anatase	anatase	1100-1200	55-60

▲ Tab. 2

Summary of sample characterization.
Sintesi dei risultati della caratterizzazioni.

The analysis indicated the pres-ence of following elements: Cu, Ti, C and O. The binding energy (BE) of Ti ($2p_{3/2}$) was the same as that of titanium dioxide at 458.6 eV in good agreement with literature [27-31]. The O(1s) peak showed only a component with BE 529.7 eV attributed to oxygen bonded to titanium and copper [28, 30, 32]. The same results were observed for the other samples of TiO_2 on copper (samples 1, 2, 4 and 5).
The simultaneous presence of copper and titanium oxide on the surface of the samples suggests that the surface structure of the samples is characterized by the presence of islands of TiO_2 and not of a continuous film. It is possible also that copper atoms or small copper moieties can migrate along the grain boundaries of the TiO_2 film. In a previous work [33] it was found that the introduction of oxy-gen with a pressure of up to $2.3x10^{-6}$ Pa, or operating at a temperature lower than 690 K at ambient pressure ($2x10^{-7}$ Pa) was sufficient to prevent segregation of copper on titanium thin films; however, migration cannot be ruled out in the present experimental conditions.
The XRD analysis did not show well defined difftaction peaks attributable to one of the several forms of titanium oxide; apparently, the TiO_2 islands were amorphous or too small to be detected with this technique. Fig. 2 (a) shows the Raman spectrum of one of the TiO_2 films (sample 3) coated on copper. Titanium dioxide crystallizes in two different tetragonal structures, anatase and rutile. Anatase be-longs to the space group D4h [34] with two unit-cell and with six Raman active modes, whereas rutile belongs to the space group D4h [34] with four Raman active modes, as reported in Tab. 3. Brookite, another form of TiO_2 with lower symmetry, is orthorombic (space group D2h [34]) with a quite com-plex Raman spectrum. The predicted Raman active modes are 36; however, the prominent Raman bands are observed at 128, 153, 247, 366 and 636 cm^{-1}.
The Raman spectra of the TiO_2 thin films deposited on copper showed a very intense band at 152 cm^{-1}, together with other bands at higher frequencies (Tab. 3) that could be identified as the intense Ra-man bands of anatase. The presence of rutile or brookite could be ruled out, because the most intense bands of rutile at 447 and 616 cm^{-1} and of brookite at 128 and 247 cm^{-1} were not detected. However, the observed Raman bands (Fig. 4a) are significantly shifted at higher energies with respect to the fre-quencies of bulk anatase. Variations in the Raman frequencies of anatase were previously observed; for example, an air-dried film showed the most intense peak shifting to 155 cm^{-1} [35]. Upshifting and broadening of the Raman bands of anatase in nanocrystalline samples were attributed to the non-stoichiometry of the material [36] or to decrease in the particle size [37], in agreement with the XRD results. The crystalline structure seems not to be correlated to a well defined deposition parameter.
As shown in Fig. 2(a), the examined TiO_2 film exhibits weak anatase peaks; moreover, copper(I) oxide with its peak at 220

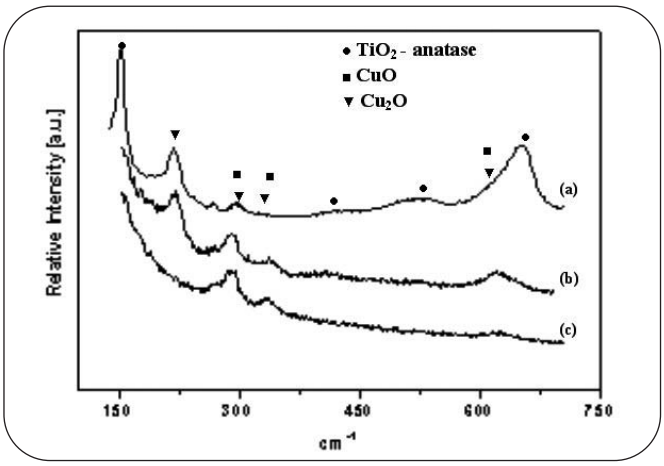

▲ Fig. 2

Raman spectra of sample 3 (a), of Cu(I) oxide [34, 35] (b) and of Cu(II) oxide [36, 37] (c).
Spettri Raman dei campioni sample 3 (a), dell'ossido di Cu(I) [34, 35] (b) and dell'ossido di Cu(II) [36, 37] (c).

Raman frequency [cm^{-1}] of Anatase [11]	Symmetry species of Anatase	Raman frequency [cm^{-1}] of Rutile [11]	Symmetry species of Rutile	Raman frequency [cm^{-1}] of Brookite [11]	Symmetry species of Brookite	Raman frequency [cm^{-1}] of coatings on copper
				128 s	Ag	
144 vs	Eg	143 w	B1g	153 vs	Ag	152 vs
197 w	Eg	247 w	B1g+ B1g	247 m	Ag	
400m	B1g	447 s	A1g	366 w	B2g	415 w
507 m	A1g					505 m
519 m	B1g					520 m
640 s	Eg	616 m	A1g	636 s	Ag	650 s
		826 w	B2g			

Tab. 3

Raman bands of titanium dioxides.

Bande Raman del diossido di titanio.

cm^{-1} [38] is detected. As a comparison, the Raman spectra of Cu(I)2O [39, 40] and of Cu(II)O [41, 42] are shown in Fig. 2 (b) and 2 (c), respectively.

The sample 1 was prepared with a mixture of gas (24% Ar, 76% O2) in comparison with other sam-ples prepared with an atmosphere containing only oxygen. It shows the lowest deposition rate (6-8 nm/min) in comparison with other samples (Tab. 1 and 2). This fact suggests that the deposition rate depends on the gas composition. The sample 3 was prepared with a bias of 50 V in comparison with other samples prepared with a bias of 120 V (2, 4 and 5). This sample shows very low deposition rate (28-33 nm/min), suggesting that also the bias influences the deposition rate.

The deposition rates for these samples (Table 1) appear reasonably high, but in no case it was possible to obtain a coating that didn't show a copper peak in XPS spectra. It may be supposed that this fact is due to the presence of a large amount of surface defects (holes, scares, etc.) of the copper substrate probably occurred during the surface preparation (Fig. 3 (a)) and/or a not uniform ionic activation of substrate surface by oxidizing plasma in the first steps of the process.

TiO_2 on stainless steel

Stainless steel is a harder material and easier to polish than copper, allowing for a better reproducibility of surface roughness. Preliminary AISI 304L stainless steel samples were coated using the deposition parameters reported in Tab. 1 (samples 6 and 7). The analysis of SIMS depth profiles of the two samples on stainless steel shows that the thickness of the TiO_2 coating is about 350-400 nm for sam-ple 6 and 250-300 nm for sample 7.

The XPS spectrum of sample 6 is shown in Fig. 1 (b). The XPS analysis of the surface of sample 6 indicated the presence of the following elements: Na, Ca, Pb, Ti, C, O. The XPS data showed the pres-ence of titanium dioxide on the sample surface. The peak of Ti(2p3/2) at BE 458.5 eV is ascribed to TiO_2 [27-31]. The fitting of O(1s) peak showed two components, the first one with BE 529.9 eV at-tributed to oxygen bonded to titanium [28, 30, 32], and the second one at BE 532.1 eV attributed to oxygen of carbonates arising from surface contamination [28-30].

The C(1s) peak showed two components, too. The main one, with BE 285 eV, corresponds to aliphatic carbon [28, 30], while the second one, with BE of 287.4 eV, is relative to carbonates due to surface contaminations [28, 30]. It was possible to find very

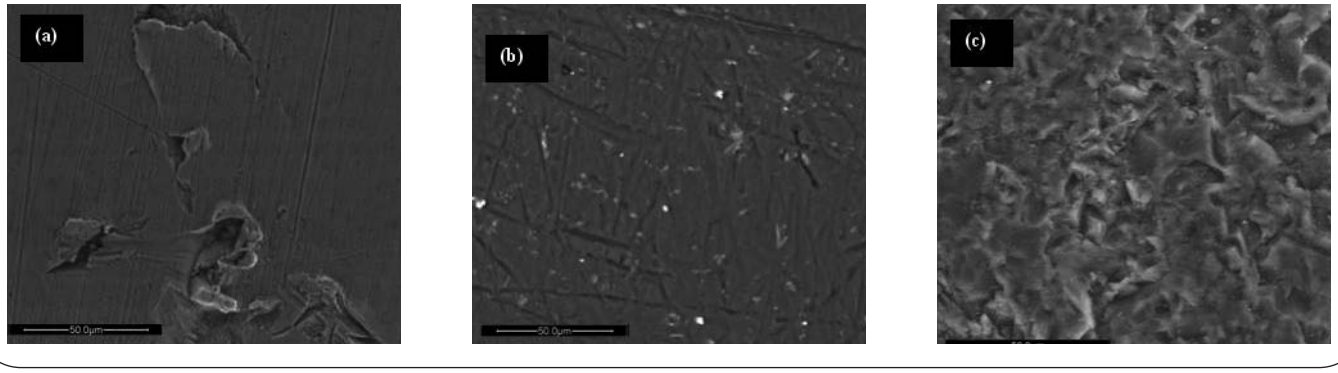

Fig. 3

Secondary electrons micrographs of the surface of TiO_2 samples on copper (sample 3) (a), stainless steel (sample 6) (b) and glass (sample 10B) (c).

Immagini in elettroni secondary della superficie dei campioni di TiO_2 su rame (sample 3) (a), acciaio inox (sample 6) (b) e vetro (sample 10B) (c).

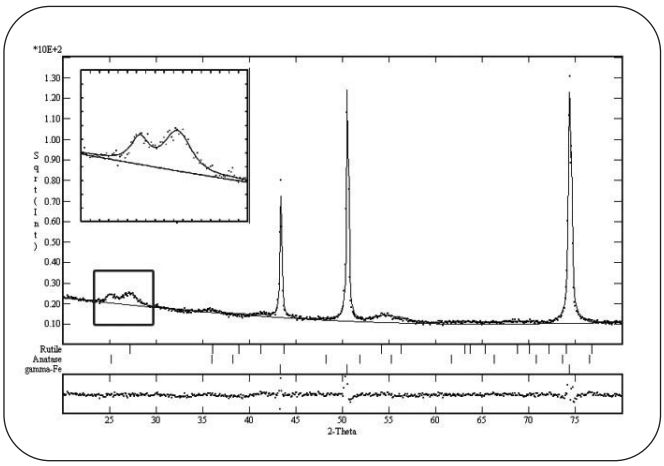

Fig. 4

X-ray diffraction pattern and Rietveld's fitting (symbols: observed, line: calculated and lower symbols: difference) for sample 6 (TiO_2 on stainless steel). In the square box a magnification of the fitting of the most intense peaks of rutile and anatase is shown.

Pattern di diffrazione e fitting mediante metodo di Rietveld per il campione sample 6 (TiO_2 on stain-less steel). Nel riquadro è stato inserito l'ingrandimento della zona dove si trovano I picchi più intensi del rutilo e dell'anatasio.

weak peaks relative to Ca(2p3/2) with BE 347 eV and Na(1s) with BE 1071.5 eV in the form of carbonates as contamination elements [28]. Finally, we observed the presence of a Pb(4f7/2) peak with BE of 138.1 as probably oxide or carbonate [28], in low concentration. The XPS analysis of the surface of sample 7 shows the same results.

The XPS data did not show the presence of substrate elements, in particular Fe, Cr and Ni. Apparently, the coatings on stainless steel are more homogeneous than those produced on copper. It may be hy-pothesised that this fact is related to the better surface uniformity in comparison with copper. In fact the micrographic examination (Fig. 3 (b)) shows no relevant defects on the surface of coated sam-ple. Moreover, chemical factors may prevent iron moieties

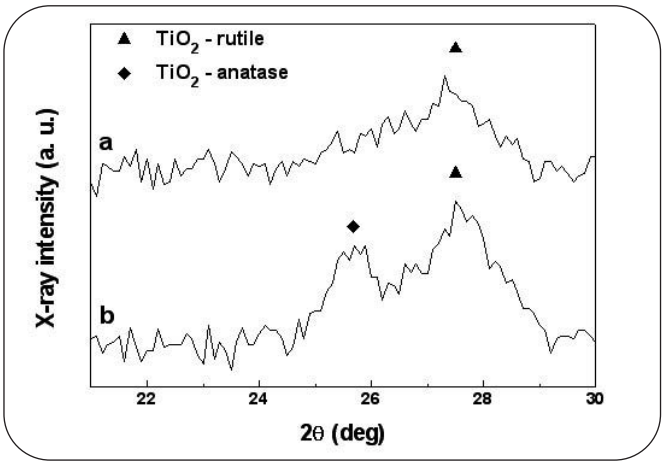

Fig. 5

Glancing angle X-ray diffraction patterns, obtained with a constant incident angle of 5°, for samples 7 (a) and 6 (b).

Pattern di diffrazione ottenuti con tecnica XRD ad angolo radente di 5° per i campioni samples 7 (a) e 6 (b).

to migrate along the TiO_2 grain boundaries at the same speed as for copper.

X-ray diffraction pattern and Rietveld's fitting for sample 6 is shown in Fig. 4. High intensity peaks of the steel substrate can be observed; moreover, in the range 20° – 30° weak peaks attributable to the coating are present. Additional X-ray diffraction analysis was performed in glancing angle configura-tion, using a constant incident angle of 5°. The 20 to 31° part of the full patterns obtained for samples 6 and 7 are shown in Fig. 5. For sample 6 two peaks are observed, one at about 25.6°, which can be ascribed to the (101) diffraction peak of anatase, and the other at about 27.5°, which can be ascribed to the (110) peak of rutile, as also reported in the literature [43, 44]. For sample 7, only one peak, belong-ing to rutile, was present. The mean crystallite size of TiO_2 was evaluated by using the Rietveld method and resulted to be of the order of a few nanometres for both samples.

The obtained results suggest that increasing the oxygen pressure tends to decrease the deposition rate, as also observed by other authors [45]. Moreover, also the EMCAS configuration seems to influence the deposition rate, with C configuration producing the smaller rate. When the deposition rate is about 20 nm/min, both rutile and anatase can be obtained, suggesting that the decrease of deposition rate is favourable for the formation of anatase.

TiO_2 on stainless steel and glass

The coatings of samples 8, 9 and 10 were produced on stainless steel and glass substrates using, for each set of samples, the same deposition parameters, as reported in Table 1. The analysis of SIMS depth profiles (Fig. 6 (a), (b) and (c)) of the three samples on stainless steel allowed us to estimate the thickness of the coatings (sputter rate was about 12 nm/min). The thickness of the TiO_2 coating was about 400-450 nm for samples 8, 750-800 nm for samples 9 and 1100-1200 nm for samples 10.

The XPS spectrum of sample 8A is shown, as an example, in Fig. 1 (c). The XPS analysis of the sur-face of sample 8A indicated the presence of the following elements: Na, Ca, Ti, C, O. The XPS data showed the presence of titanium dioxide on the sample surface. The peak of Ti(2p3/2) at BE 458.5 eV is ascribed to TiO_2 [27-31]. The fitting of O(1s) peak showed two components, the first one with BE 529.9 eV attributed to oxygen bonded to titanium [28, 30, 32], and the second one at BE 532.1 eV at-tributed to oxygen of carbonates arising from surface contamination [28-30].

The C(1s) peak showed two components, too. The main one, with BE 285 eV, corresponds to aliphatic carbon [28, 30], while the second one, with BE of 287.4 eV, is relative to carbonates due to surface contaminations [28, 30]. It was possible to find very weak peaks relative to Ca(2p3/2) with BE 347 eV and Na(1s) with BE 1071.5 eV in the form of carbonates as contamination elements [28]. We ob-tained the same results for the samples 9A and 10A on stainless steel and 8B, 9B and 10B on glass. It was possible to obtain homogeneous coatings on glass, too. Microscopy analysis of the surface coat-ings on glass shows no relevant defects, as depicted in Fig. 3 (c). SIMS data showed the presence of Ca, Na, K and Mg as superficial contamination but with an amount three orders of magnitude lower than the titanium content. The surface analysis did not show the presence of relevant amounts of elements such as Fe, Cr and Ni coming from the substrate.

The X-ray diffraction pattern of sample 10B (TiO_2 on glass), collected in Bragg-Brentano configura-tion, showed as the main feature the broad hump characteristic of the amorphous glass structure pre-sent in the range between 20° and 30°; very small peaks belonging to the coating are superimposed to the hump. An additional X-ray diffraction analysis was performed in glancing angle configuration, by using a constant incident angle of 10°. Only

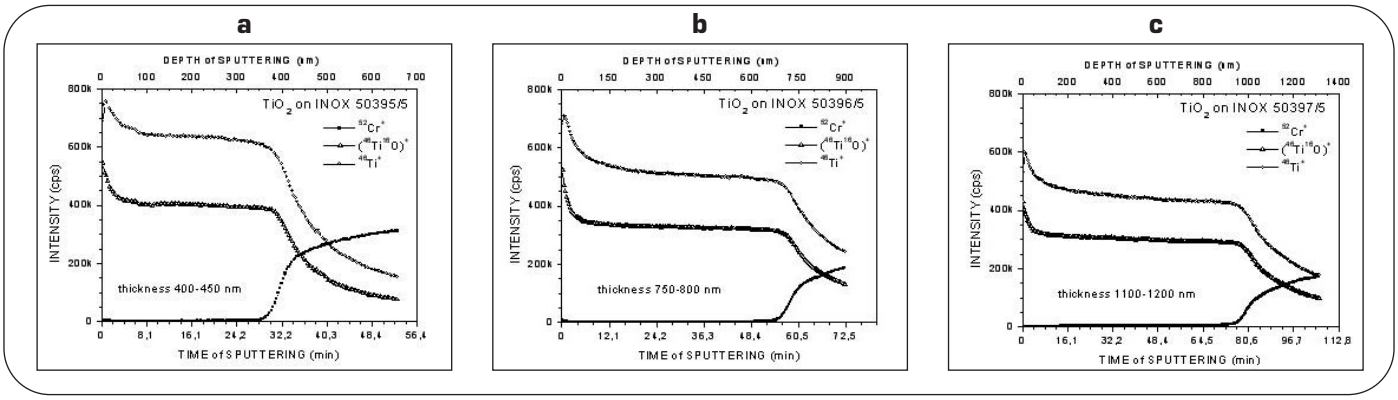

Fig. 6

SIMS depth profiles for samples 8A (a), 9A (b) and 10A (c) (TiO_2 on stainless steel).

SIMS depth profile dei campioni samples 8A (a), 9A (b) e 10A (c) (TiO_2 su acciaio inox).

anatase was detected in the coatings, as shown in Fig. 7 (a). This result should be compared with that obtained for sample 10A (TiO_2 stainless steel), where only rutile was detected (Fig. 7 (b)) [43, 44].

MicroRaman analysis on samples 8B, 9B and 10B (TiO_2 on glass) are reported in Fig. 8. All the spec-tra show an intense peak at 142 cm^{-1}. In Fig. 8 (a) two wide peaks attributable to the amorphous titania are observed. In spectra (b) and (c) it can be noted the presence of three peaks at 396, 519 and 635 cm^{-1}. It can be asserted that the crystalline structure of TiO_2 on samples 9B and 10B is anatase, while the Raman spectrum of sample 8B can be attributed to the presence of both amorphous and crystalline (anatase) TiO_2 [34-38].

Sample	Substrate	Irradiation time	$\Delta C^{[a]}$
8B	Glass	5 h	–10%
		24h	–23%
		30h	–29%
		55h	–38%
8A	Stainless steel	5 h	–4%
		24h	–8%
		30h	–11%
		55h	–24%
9B	Glass	3h	–7%
		22h	–55%
		48h	–72%
9A	Stainless steel	21h	–6%
		45h	–25%
10B	Glass	5h	–11%
		24h	–52%
		48h	–73%

Tab. 4

Results of the photocatalytic experiments. ([a] Relative change (%) of the phenol concentration; the initial concentration was $1.0x10^{-4}$ M)

Risultati degli esperimenti di fotocatalisi. ([a] Variazione relativa (%) della concentrazione di fenolo; la concentrazione iniziale era $1.0x10^{-4}$ M)

Raman spectra of samples 8A, 9A and 10A (TiO_2 on stainless steel) are shown in Fig. 9. In all the spectra two intense peaks at 445 and 613 cm–1 and two broad peaks at lower intensity at 156 and 255 cm^{-1} can be observed; the peaks are attributable to rutile, in good agreement with the literature [34-38].

Samples 8, 9 and 10 were prepared with the same deposition parameters, increasing the time of deposi-tion only, as described in Tab. 1. The increasing of deposition time leads to a small increase of depo-sition rate, as shown in Tab. 2, due to an initial inertness of the deposition process in this condition. In this case it is the substrate that seems to influence mainly the crystalline structure of the TiO_2 coat-ings, also in accordance with literature [46]: the TiO_2 coatings on stainless steel show the typical struc-ture of rutile, while the coatings on glass show the typical structure of anatase. This substrate effect may be due to many factors, as the different lattice mismatch of anatase and rutile at different substrates, the different electrical conductivity of the substrates that influences the effect of bias and the different thermal conductivity of the substrates during the condensation process.

After 10 minutes of deposition, the TiO_2 coating on glass shows both amorphous and crystalline struc-ture (anatase) while the coating on stainless steel shows the rutile crystalline structure. The thin TiO_2 films have a bigger structural disorder than the thicker TiO_2 films when they grow directly on amor-phous glass substrates as also observed by other authors [47].

After 20 minutes of deposition, the XRD patterns show the presence of a (101) narrow diffraction peak of anatase (Fig. 7 (a)) and a (111) spread diffraction peak of rutile (Fig. 7 (b)). The narrow peak suggests a greater crystallite size of the anatase coating than the rutile one. It may be hypothesised that TiO_2 crystal growth tends to prevail on glass in comparison with stainless steel. In fact greater crystal-lite size corresponds to longer time of crystal growth [48].

Photocatalitic activity of the TiO_2 coatings

The photocatalytic activity of the samples was investigated by studying the degradation of a target molecule, phenol, dissolved in an aqueous solution in contact with the coating. The sample was irradi-ated with UVA light, which is exclusively absorbed by the TiO_2 coating. The examined samples were 8 and 9 on both glass (B) and stainless steel (A) as substrates, and 10B on glass. The results of the pho-tochemical experiments are reported in Tab. 4. Fig. 10 shows, as an example, the luminescence spec-tral changes of a phenol solution exposed to sample 9B on glass as a function of the coating irradia-tion time.

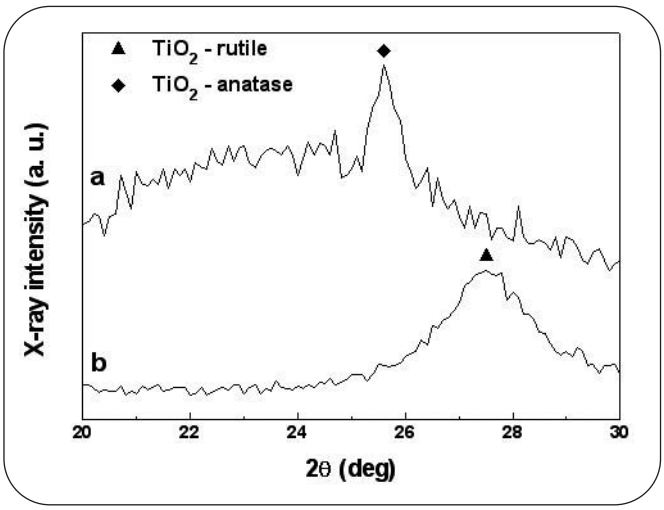

Fig. 7

Glancing angle X-ray diffraction patterns, obtained with a constant incident angle of 10°, for samples 10B (TiO_2 on glass) (a) and 10A (TiO_2 on stainless steel) (b).

Patterns di diffrazione ottenuti con tecnica XRD ad angolo radente di 10° per i campioni samples 10B (TiO_2 su vetro) (a) and 10A (TiO_2 su acciaio inox) (b).

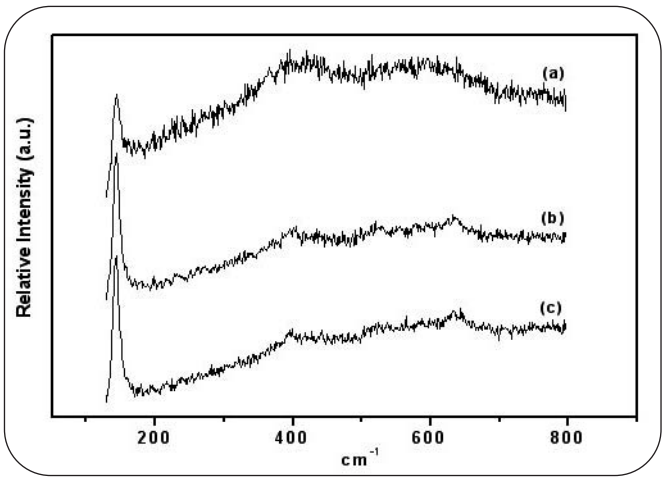

Fig. 8

MicroRaman spectra of samples 8B (a), 9B (b) and 10B (c) (TiO_2 on glass).

Spettri MicroRaman dei campioni samples 8B (a), 9B (b) e 10B (c) (TiO_2 su vetro).

The coatings deposited on glass exhibited a good photocatalytic activity, whereas those on stainless steel show a low photoactivity. The modest photoactivity of the coatings on steel can be ascribed to the presence of the low activity rutile phase [8]. Conversely, the anatase phase of the coatings on glass resulted to provide good activity.

The comparison of the results obtained for samples 9B and 10B, which differ only for the thickness of the coating, is particularly interesting. The fact that they showed the same photocatalytic activity indi-cates that the TiO_2 thickness is not a crucial parameter, at least for thicknesses larger than 750 nm. In fact, it has to be considered that if the coating is porous, i.e. has channels and cavities that can be en-tered by the targeted molecules, photodegradation can occur in the TiO_2 bulk and the thickness is ex-pected to affect the photocatalytic activity. Conversely, if the coating is not porous the photoreaction can take place only on the surface and thickness will not be important: only roughness will matter. Furthermore, layer of TiO_2 of a few hundreds of nm thickness absorbs completely the incident light for $\lambda<370$ nm, as shown by spectrophotometric measurements. Therefore it can be expected that a fur-ther increase in the thickness of the sample – irrespective of its porosity – will not lead to an improve-ment in the photoactivity, because the light cannot penetrate deep into the

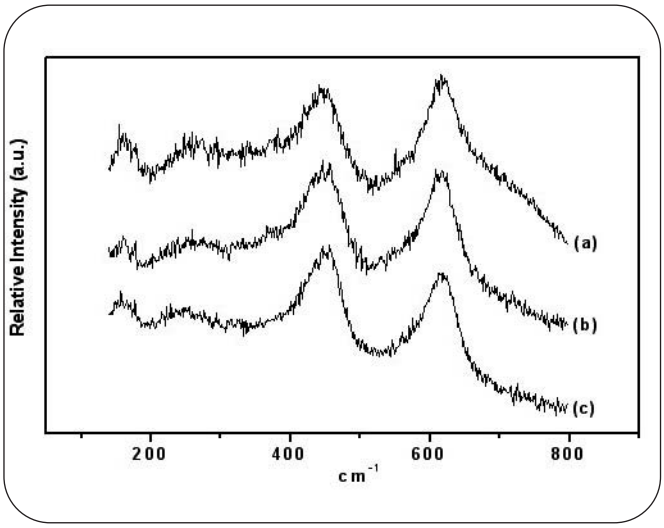

Fig. 9

MicroRaman spectra of samples 8A (a), 9A (b) and 10A (c) (TiO_2 on stainless steel).

Spettri MicroRaman dei campioni samples 8A (a), 9A (b) e 10A (c) (TiO^2 su acciaio inox).

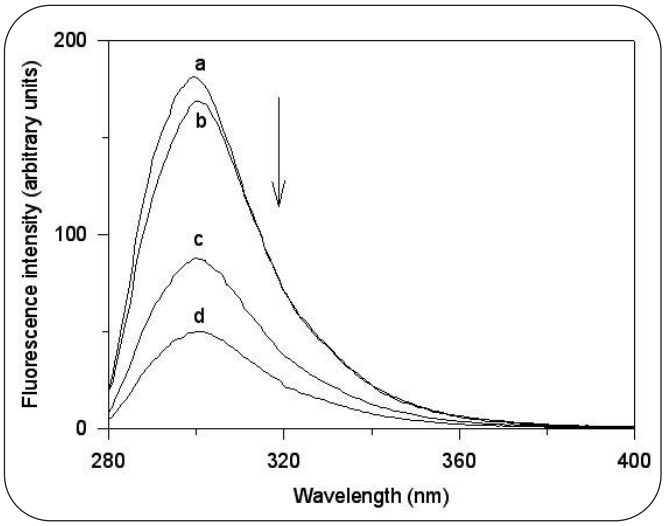

Fig. 10

MicroRaman spectra of samples 8A (a), 9A (b) and 10A (c) (TiO_2 on stainless steel).

Spettri MicroRaman dei campioni samples 8A (a), 9A (b) e 10A (c) (TiO_2 su acciaio inox).

coating. The smaller pho-toactivity of sample 8 on glass may be ascribed to the presence of amorphous TiO_2 besides anatase and/or the smaller thickness (400-450 nm).

CONCLUSION

Titanium dioxide coatings were prepared on various substrates by means of a modified electric-arc physical vapour deposition (EA-PVD) technique. The coatings were chemically and structurally char-acterized. The deposition parameters were varied in the attempt of preparing coatings with TiO_2 in the anatase form, i.e. that might exhibit good photocatalytic properties. The characteristics of the coatings depend on both substrate type and deposition parameters. The crystal structure is influenced mainly by substrate composition (copper (anatase), stainless steel (rutile) and glass (anatase)) and the change of substrate type seems also to affect the crystalline size of coating grains. The crystalline structure may be also influenced by the deposition rate, with lower rates that tend to favour the anatase forma-tion. The deposition rate of the coatings seems to be influenced by many deposition parameters, mainly gas composition, gas pressure, bias and EMCAS configuration; the substrate heating does not seem to alter the characteristics of the coating as the other parameters. The photochemical experiments performed on some of the most promising samples show that the crystalline form of the TiO_2 coating is a main factor in determining the photoactivity. The anatase coatings are able to degrade photocata-lytically and rapidly the phenol solution in comparison with rutile coatings. The influence of the thick-ness of the coatings was also investigated, and it was found that the increase in thickness above about 700 nm does not lead to an improvement of the photocatalytic action.

ACKNOWLEDGMENTS

This work was supported by the Region Emilia-Romagna through the PRIITT program (Misura 3.1 Azione A - contract nr. 250).

BIBLIOGRAPHY

[1] N. Berger-Keller, G. Bertrand, C. Filiatre, C. Meunier, C. Coddet, Surf. Coat. Technol. 168 (2003) 281
[2] Meng Ni, Michael K.H. Leung, Dennis Y.C. Leung and K. Sumathy, Renew. Sust. En. Rev. 11 (2007) 401
[3] M.R. Hoffmann, S. T. Martin, W. Choi and D. W. Bahnemann, Chem. Rev. 95 (1995) 69
[4] A. Mills and S.K. Lee, J. Photochem. Photobiol. A: Chemistry 152 (2002) 233
[5] A. Fujishima, Tata N. Rao and D. A. Tryk, Electroc. Acta 45 (2000) 4683
[6] S. Hata, Y. Kai, I. Yamanaka, H. Oosaki, K. Hirota, S. Yamazaki, JSAE Review 21 (2000) 97
[7] N. Negishi and K. Takeuchi, Materials Letters 38 (1999) 150
[8] M.A.Fox, M.T.Dulay, Chem. Rev. 93 (1993) 351
[9] J. Yu, X. Zhao, Q. Zhao, Mater. Chem. Phys. 69 (2001) 25
[10] C. J. Taylor, D. C. Gilmer, D. G. Colombo, G. D. Wilk, S. A. Campbell, J. Roberts, W. L. Glad-felter, J. Am. Chem. Soc. 121 (1999) 5220
[11] M. Ritala and M. LeskeläErja Nykänen, P. Soininen, L. Niinistö, Thin solid Films 225 (1993) 288
[12] G. Thorwarth, S. Mändl, B. Rauschenbach, Surf. Coat. Technol. 128 (2000) 116
[13] Y. Choi, S. Yamamoto, T. Umebayashi, M. Yoshikawa, Solid State Ionics 172 (2004) 105
[14] P.Zemanand, S.Takabayashi, Thin Solid Films 433 (2003) 57
[15] B. Kepenek, U.Ö.fi. fieker, A. F. Çak›r, M. Ürgen, C. Tamerler, Key Engin. Mater. 254 (2004) 463
[16] Guan-Jun Yang, Chang-Jiu Li, Feng Hana, Akira Ohmori, Thin Solid Films 466 (2004) 81
[17] J. R. Davis, Handbook of Thermal Spray Technology, ASM International, 2004
[18] European Patent Application EP 1 624 087 A1
[19] A. Lavacchi, B. Cortigiani, G. Rovida, U. Bardi, A. Atrei, R. Angelucci, L. Dori, S. Nicoletti, A. Poggi, Sens. Actuators B 71 (2000) 123
[20] E. Galvanetto, F.P. Galliano, F. Borgioli, U. Bardi and A. Lavacchi, Thin Solid Films 384 (2001) 223.
[21] A. Tolstogouzov, S. Daolio, C. Pagura, Surf. Sci. 441 (1999) 213.
[22] A. Tolstogouzov, S. Daolio, C. Pagura, Nucl. Instrum. Meth. B 183 (2001) 116.
[23] A. Tolstogouzov, S. Daolio, C. Pagura, C.L.Greenwood, Int. J. Mass Specrom. 214 (2002) 327.
[24] L. Lutterotti, S. Matthies, H.-R. Wenk, in: J.A. Szpunar (ed.), Proc. of the 12th International Con-ference on Textures of Materials (ICOTOM-12), Vol. 1, NRC Research Press, Ottawa, (1999), 1599
[25] M. Montalti, A. Credi, L. Prodi, M. T. Gandolfi, Handbook of Photochemistry, 3rd Ed., CRC Press, Boca Raton, 2006, Ch. 10
[26] H. Hidaka, H. Kubota, M. Graetzel, E. Pelizzetti, N. Serpone, J. Photochem. 1986, 35, 219-230
[27] A.F. Carley, P.R.Chalker, J.C. Riviere, M.W.Roberts, J. Chem. Soc. Faraday Trans. 1 83 (1987) 351
[28] C. D. Wagner, W. M. Riggs, L. E. Davis, and J. F. Moulder, Handbook of X-ray Photoelectron Spectroscopy (G. E. Muilenberg, editor), Perkin-Elmer Corporation (Physical Electronics), 1979 (1st edition)
[29] C. D. Wagner, Surf. Interf. Anal. 3 (1981) 211
[30] R.A. DiFelice, J.G. Dillard, D. Yang, Int. J. Adhesion and Adhesives 25 (2005) 277
[31] H. Han, L. Zan, J. Zhong, L. Zhang and X. Zhao, Mater. Sci. Engin. B, 110 (2004) 227
[32] Y. Chen and D. Dionysiou, Applied Catalysis B: Environmental, 62 (2006) 255
[33] M. Yoshitake and K. Yoshiara, Applied Surface Science 100/101 (1996) 203
[34] G. A. Tompsett, G.A. Bowmaker, R.P. Cooney, J.B. Metson, K.A. Rodgers, J.M. Seakin, J. Ra-man Spec. 36 (1995) 57.
[35] T. L. Hanley, V. Luca, I. Pickering, R. F. Howe, J. Phys. Chem. B 106 (2002) 1153
[36] Y. Djaoued, S. Badilescu, P.V. Ashrit, J. Robichaud, Int. J. Vibr. Spectrosc. 5 (2001) 4
[37] H. C. Choi, Y. M. Jung, S. B. Kim, Vibr. Spectrosc. 37 (2005) 33
[38] A. Kudelski, B. Pettinger, Surf. Science 566-568 (2004) 1007
[39] http://www.aist.go.jp/RIODB/db092/reagents_data/abcde/pdf_data/cu002.pdf
[40] Y. Petrof, P. Y. Yu,Y. R. Shen, Physical Review 12 (1995) 1075

[41]http://www.aist.go.jp/RIODB/db092/reagents_data/abcde/pdf_data/cu001.pdf
[42] J. F. Xu, W. Ji, Z. X. Shen, S. H. Tang, X. R. Ye, D. Z. Jia, X. Q. Xin, Journal of Solid State Chemistry 147 (1999) 516
[43] JCPDS card n° 21-1272, Powder Diffraction File, Joint Committee on Powder Diffraction Stan-dards, International Centre for Diffraction Data, Swarthmore, PA (USA), 1992.
[44] JCPDS card n° 21-1276, Powder Diffraction File, Joint Committee on Powder Diffraction Stan-dards, International Centre for Diffraction Data, Swarthmore, PA (USA), 1992.
[45] V. Vancoppenolle, P. -Y. Jouan, M. Wautelet, J. -P. Dauchot and M. Hecq, Surf. Coat. Technol. 116-119 (1999) 933-937
[46] L. Bárdo and H. Baránková, Surf. Coat. Technol. 146-147 (2001) 463-468
[47] P. Zeman and S. Takabayashi, Thin Solid Films 433 (2003) 57-62
[48] Donald L. Smith, Thin Film Deposition - Principles and Practice, Ed. McGraw-Hill, 2005

ABSTRACT

RIVESTIMENTI SOTTILI DI TiO_2 PREPARATI MEDIANTE ELECTRIC ARC-PHYSICAL VAPOUR DEPOSITION

Parole chiave: rivestimenti, processi, ea-pvd, spettroscopia, caratterizzazione materiali

Il Biossido di titanio è un materiale multifunzionale con numerose potenziali applicazioni nel campo della tecnologia medica, dei sensori a gas e di protezione dall'usura, a causa delle sue caratteristiche (stabilità fisica e chimica e non tossicità). Come materiale semiconduttore, il biossido di titanio ha sollevato un grande interesse per le sue proprietà fisico-chimiche, che hanno portato a numerose applicazioni industriali. L'eccitazione di TiO_2 con fotoni con energia uguale o superiore al suo band-gap conduce alla promozione di elettroni nella banda di conduzione e la concomitante formazione di vacanze nella banda di valenza. Tali coppie fotogenerate elettrone-vacanza possono causare reazioni di ossidoriduzione che possono avvenire sulle specie chimiche adsorbite sulla superficie del semi conduttore. Il grande potere ossidante delle vacanze fotogenerate, l'inerzia chimica e la mancanza di tossicità sono i motivi principali per il diffuso utilizzo della TiO_2 come fotocatalizzatore. In questo lavoro, rivestimenti sottili di TiO_2 sono stati deposti su vari substrati, attraverso l'evaporazione di un target di titanio metallico in atmosfera ossidante mediante un impianto industriale modificato Electric Arc-Physical Vapour Deposition (EA-PVD).
I rivestimenti sono stati caratterizzati chimicamente (mediante XPS e SIMS) e dal punto di vista cristallografico (mediante spettroscopia Raman e XRD). È stato possibile preparare rivestimenti di TiO_2 con diversa struttura cristallina e spessore su substrati di diversa composizione. È stato messo a punto un dispositivo per valutare l'attività fotocatalitica dei campioni durante irraggiamento UVA, utilizzando il fenolo come molecola target in soluzione acquosa. Gli esperimenti di fotodegradazione effettuati su alcuni dei più Promettenti campioni hanno dimostrato che la forma cristallina della TiO_2 è il principale fattore che determina l'attività fotocatalitica. I rivestimenti di anatasio sono stati in grado di fotodegradare il fenolo in soluzione molto più veloce rispetto ai rivestimenti di rutilo.